ISSN 0001-4370, Oceanology, 2023, Vol. 63, Suppl. 1, pp. S202–S214. © Pleiades Publishing, Inc., 2023.

MARINE BIOLOGY

Development of a Maximum Specific Photosynthetic Rate Algorithm Based on Remote Sensing Data: a Case Study for the Atlantic Ocean

A. S. Malysheva[a, b, *], P. V. Lobanova[a], and G. H. Tilstone[c]

[a] *St. Petersburg State University, St. Petersburg, 199034 Russia*

[b] *Nansen International Environmental and Remote Sensing Center, St. Petersburg, 199034 Russia*

[c] *Plymouth Marine Laboratory, Plymouth, PL1 3DH United Kingdom*

**e-mail: alexandra.malysheva@niersc.spb.ru*

Received July 31, 2023; revised September 27, 2023; accepted September 28, 2023

Abstract—New regional empirical algorithms were developed to obtain maximum specific photosynthetic rates of phytoplankton (P_m^B) in the surface layer of the Atlantic Ocean. These algorithms were based on the dependence of P_m^B on seawater temperature. Sea Surface Temperature remote sensing data and the PANGAEA global database of photosynthesis–irradiance parameters were used to test the algorithm. In addition, the variability in P_m^B, both spatially (from 60° S to 85° N) and seasonally, (2002–2013) was estimated. The highest P_m^B was obtained in December in areas of deep convection and the interaction between the Labrador Current and the Gulf Stream, while minimum values were observed in the northern and equatorial–tropical parts of the ocean during the time intervals between the phytoplankton blooms (March to September–October). In addition, existing P_m^B and P_{opt}^B algorithms used in primary production models, as well as the P_m^B algorithm developed using temperature and chlorophyll *a* data from AMT-29, which were then tested using the PANGAEA dataset. The results show that the new P_m^B algorithm developed using seawater temperature data with regionally adjusted empirical coefficients correlated best with the in situ data.

Keywords: primary production, chlorophyll *a*, assimilation number, phytoplankton blooms, Atlantic Ocean

DOI: 10.1134/S000143702307010X

INTRODUCTION

The specific maximum rate of photosynthesis or assimilation number (P_m^B) is a necessary component of many primary production (PP) models, because this parameter of the photosynthesis illumination curve characterizes the photosynthetic response of marine phytoplankton to light saturation [21]. In the Global Ocean, P_m^B varies over a wide range: from 1 to 24 mgC (mgChl *a*)$^{-1}$ h^{-1}, where Chl *a* is chlorophyll *a*. Minimum P_m^B values are typical of high latitudes and central parts of the Subtropical Gyres, whilst maximum P_m^B values are found in coastal communities, subtropical and tropical waters [5, 17]. In general, the experimental determination of P_m^B conducted at sea is limited in both space and time [9], and it is therefore hard to describe the interannual and seasonal trends in P_m^B for the entire Global Ocean. However, long-term measurements of P_m^B have been undertaken in specific areas of the ocean. For example, in the Black Sea, at a distance of 2 km from the city of Sevastopol, a long time series has been collected which shows that the highest P_m^B was at the end of spring–beginning of summer (up to 14 mgC (mgChl *a*)$^{-1}$ h^{-1}) during a diatom bloom, whereas in autumn, when pyrrophyta algae are predominant, its values become somewhat lower (up to 8 mgC (mgChl *a*)$^{-1}$ h^{-1}); in winter and late summer, they are in the range of 4–12 mgC (mgChl *a*)$^{-1}$ h^{-1}) [1]. In coastal and shelf waters of Nova Scotia, Canada, the highest P_m^B values were recorded in July–August (6–12 mgC (mgChl *a*)$^{-1}$ h^{-1}), and the minimum values occurred in the cold period of the year (from January to March) (3–4 mgC (mgChl *a*)$^{-1}$ h^{-1}) [17]. An increase in P_m^B precedes a marine phytoplankton bloom; the time interval between these events can be a month [1].

There can be considerable variation in P_m^B which is associated with fluctuations in the annual primary production cycle of marine phytoplankton [5, 19]. The parameter is normalized to biomass (index *B*), so that the phytoplankton biomass involved in photosynthesis

is accounted for [5, 20, 25]. However, Obtaining accurate P_m^B remains one of the main obstacles in determining PP using models and remote sensing data [7, 8, 14, 23]. Due to the difficulty in obtaining the shipborne *in situ* photosynthetic parameter data, current algorithms that account for the influence of environmental conditions are used. The most important factors affecting the variability in P_m^B are: solar radiation, water temperature, the supply of nutrients (N), and chlorophyll *a* content [5]. P_m^B increases with a temperature in the range from –1 to 20°C and decreases in the range from 20 to 28°C. A rapid decrease is related to the suppression of phytoplankton vital processes (increased energy costs for the photoadaptation at high irradiance in stratified oligotrophic waters) and insufficient N supply [7, 16, 28, 30]. Temperature accounts for 50–70% of the total variability in P_m^B [5, 12]; therefore, many P_m^B models are based on the dependence of this parameter on Sea Surface Temperature (SST) [6, 7, 15, 22]. Despite the fact that SST limits the physiology of photosynthetic organisms to a lesser extent compared to light and N availability, this parameter is a major predictor of photosynthetic rates and is readily available from satellite data [23]. In general, the addition of other parameters (phytoplankton biomass and N) to the P_m^B model equations leads to better correlation of model estimates with in situ data but only in certain areas (for example, the North Atlantic region [33]), and, therefore, the main emphasis is on the use of SST alone. Algorithms developed for entire ocean basins using satellite data are characterized by low or moderate correlations with in situ data ($r^2 = 0.29$, 0.21 and –0.21, respectively for P_m^B models [6, 7, 22]) [23], it therefore makes sense to compile equations for individual regions and water masses, as temperature can vary greatly not only with distance from the equator, but also in specific seas.

The objective of this study therefore is to develop regional empirical algorithms for P_m^B as a function of temperature over the entire Atlantic Ocean with different oceanographic conditions. The algorithm is validated using in situ data and compared with other algorithms available from the literature.

MATERIALS AND METHODS

Data. The variability in phytoplankton production was studied using the PANGAEA global database using parameters from photosynthesis-irradiance curves [10]: P_m^B (mgC (mgChl *a*)$^{-1}$ h^{-1}) and chlorophyll *a* concentration (mg m^{-3}) in the surface waters (0–30 m), at stations located between 60° S and 83° N in sixteen biogeographic provinces (Figs. 1b–1c). The investigation covered the period of 2002–2013. This database does not contain the in situ water temperature (°C) data and, therefore, P_m^B was obtained using the estimated satellite SST from the NASA Physical Oceanography Distributed Active Archive Center database with a time resolution of one day and a spatial resolution of 0.01° × 0.01° (JPL MUR MEaSUREs Project. 2015. v. 4.1, https://podaac.jpl.nasa.gov/dataset/MUR-JPL-L4-GLOB-v4.1). In this database, SST is normalized to a temperature of the mixed upper layer based on the in situ data. The satellite data quality was validated with the in situ SST data from the 29th Atlantic Meridional Transect (AMT-29), which was carried out from 16 October to 19 November 2019 between the UK and Punta Arenas, Chile. From the validation results, the satellite data accounted for 98% of the variability in the in situ data ($n = 20$, $r^2 = 0.98$).

The study used 350 PANGAEA stations (Fig. 1c) located in eight biogeochemical provinces to assess the spatiotemporal variability in P_m^B and to validate the algorithms. To develop the regional empirical P_m^B estimation algorithms, 141 stations (in areas 1, 3, and 4) were selected from the PANGAEA database as a test sampling dataset (Fig. 1b).

Atlantic meridional transect (AMT-29). We also used the in situ data collected on AMT-29 which included: P_m^B (mgC (mgChl *a*)$^{-1}$ h^{-1}), water temperature (°C), Chl *a* concentration (mg m^{-3}), at the stations located between 49° N and 42° S in six biogeographic provinces (Fig. 1a). The data were obtained from 20 stations in the surface horizon (5–14 m). P_m^B was determined during the research vessel run in the course of the experiment based on the method described in [34] without taking into account photoinhibition.

Study areas. The Atlantic Ocean data are distributed between the areas covering one or more biogeographical provinces according to the Longhurst province classification [20]. The classification is used to assess PP in the Global Ocean based on the physical environmental conditions (illumination, water dynamics, temperature, and salinity, gas conditions, etc.) which exert an influence on a structure and function of phytoplankton communities on a large scale, as well as on N contents and average illumination within the surface mixed layer, that affects phytoplankton physiology including photosynthetic rates and magnitude and specificity of N absorption) [9, 19]. The study was carried out in eight areas (Table 1).

Seasons. Stations were selected according to the actual season characteristic of a particular hemisphere (Fig. 1c): spring (Northern Hemisphere (NH): March–May; Southern Hemisphere (SH): September–November), summer (NH: June–August; SH: December–February), autumn (NH: September–November; SH: March–May), and winter (NH: December–February; SH: June–August).

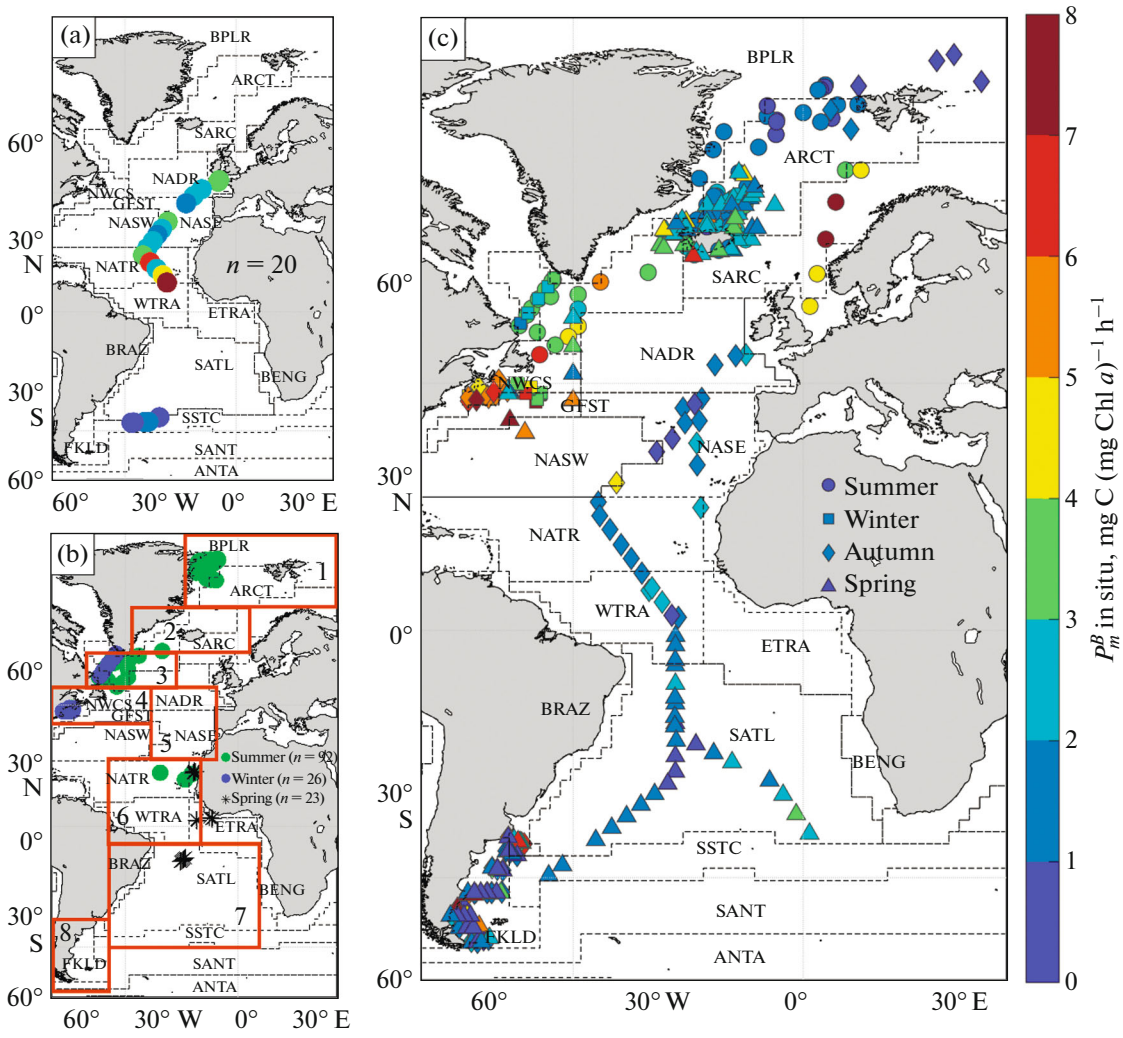

Fig. 1. Spatial distribution in the assimilation number P_m^B (mgC (mg Chl a)$^{-1}$ h^{-1}) (P_m^B scale is shown on right): (a) stations for the AMT-29 research cruise ($n = 20$); (b) test sample stations from PANGAEA ($n = 141$); areas are highlighted in brown; (c) in situ data stations from PANGAEA ($n = 350$). Boundaries of biogeographic provinces are outlined according to [20].

Algorithms for obtaining specific optimum and maximum photosynthetic rates. To verify the compliance between model values and real in situ data, several temperature algorithms for obtaining P_m^B were validated. Three P_m^B algorithms (*BF* [7], *BB* [6], and *M* [22]) using SST as a predictor were considered (Table 2). The *BB* algorithm also took a day length (DL) into account. The *BF* and *BB* algorithms were developed for the Atlantic Ocean; the *M* algorithm, a simple linear equation, was based on the data on Lake Minnetonka in North America (Table 2). P_{opt}^B, a specific optimum rate of photosynthesis, is used in *BF* and *M* instead of P_m^B. The P_{opt}^B parameter is derived for the entire euphotic zone rather than for a surface or specific depth value. It corresponds to the optimal maximum photosynthetic rate over the photic zone based on the assumption that optimum photosynthesis occurs under the point specific (station or pixel) conditions [7]. In addition, we also developed an algorithm for obtaining P_m^B using an SST and Chl *a* function from the AMT-29 data.

RESULTS

Spatiotemporal variability in P_m^B from the PANGAEA data. The seasonal variability in P_m^B in the Atlantic Ocean show that the greatest amplitude was observed in spring (Fig. 2a: 0.6–12.7 mgC (mgChl a)$^{-1}$ h^{-1}) with the maximum annual Chl *a* concentration of 2.1 mg m^{-3} and SST of 8.1°C (Table 3). In summer, the phytoplankton biomass was much lower (0.88 mg m^{-3}), and the average SST was minimum for the year, while average P_m^B was almost identical to that in spring and

Table 1. Study areas and their characteristics

Area	*N*	Provinces after A. Longhurst [20]	Bloom peak, month	Study area (PANGAEA data)	Predominant phytoplankton species after A. Longhurst [20]
1	25	BPLR, northern part of ARCT	July	June–September (2010, 2013)	Diatoms, coccolithophorids
2	129	Middle part of ARCT, western part of SARC	Bloom beginning: April–May	April–August (2003–2013)	Diatoms, coccolithophorids
3	23	Labrador Sea: southern parts of BPLR and ARCT	July	May–July (2002, 2003)	Diatoms and dinoflagellates
4	47	NWCS, GFST	April	April–May (2003), October–December (2002, 2003)	Diatoms
5	14	NADR, NASE	March–June	September–October (2004, 2010, 2012)	Diatoms
6	15	NATR, WTRA	July–September	October–November (2004, 2010, 2012)	Cyanobacteria
7	24	SATL	End of February	October–November (2004, 2012)	Cyanobacteria
8	69	Southern part of BRAZ, FKLD	November–April, peak in January	March (2006), September and October (2005, 2006)	Diatoms and cyanobacteria [31]

Table 2. P_m^B and P_{opt}^B algorithms as functions of water temperature considered in the study

Abbreviated name of algorithm	Algorithm	Accuracy, area	Reference
BF	$P_{\text{opt}}^B = -3.27\times10^{-8}T^7 + 3.41\times10^{-6}T^6 - 1.35\times10^{-4}T^5 + 2.46\times10^{-3}T^4 - 0.02T^3 + 0.06T^2 + 0.28T + 1.3$	$r^2 = 0.58$; $n = 1041$, Northwest Atlantic region	[7]
BB	$P_m^B = \frac{10\times(-0.054T + 2.21)}{DL}$	$r^2 = 0.22$; $n = 4179$, Atlantic Ocean	[6]
M	$P_{\text{opt}}^B = 0.118T + 1.25$	Lake Minnetonka (accuracy data are not available)	[22]
MY-21	$P_m^B = -1.71 + 0.22T + 0.43Chla$	$r^2 = 0.56$; $n = 20$, Atlantic Ocean (Fig. 1a), AMT-29 data	Section "Results", Eq. (1)

autumn (2.53 ± 1.79 mgC (mgChl *a*)$^{-1}$ h^{-1}; Table 3). In autumn, with a maximum average water temperature of 15.9°C and a low Chl *a* concentration (0.84 mg m^{-3}, on average), average P_m^B remained at the level of the previous seasons. In winter (December), with a minimum phytoplankton biomass (Chl *a* = 0.7 mg m^{-3}) and average SST of 6.9°C, average P_m^B was maximum (3.85 ± 1.25 mgC (mgChl *a*)$^{-1}$ h^{-1}).

The spatial variability in P_m^B showed that P_m^B was minimum (less than 1.9 mgC (mgChl *a*)$^{-1}$ h^{-1}) in cold northern waters (area 1) and in summer when there was an average Chl *a* concentration of 0.9 mg m^{-3} (Fig. 2a). To the south (area 2), the waters were warmer, there was a greater variability in Chl *a* (0–16.9 mg m^{-3}), with a predominance of coccolithophorid species, and P_m^B was higher (2.8 mgC (mgChl *a*)$^{-1}$ h^{-1}, on average), and its range was the largest of all the regions analyzed (Fig. 2b). In area 3, the water temperature increased, P_m^B was higher, the moderate phytoplankton biomass was represented by diatoms and dinoflagellates, and the measurements were carried out at the bloom peak

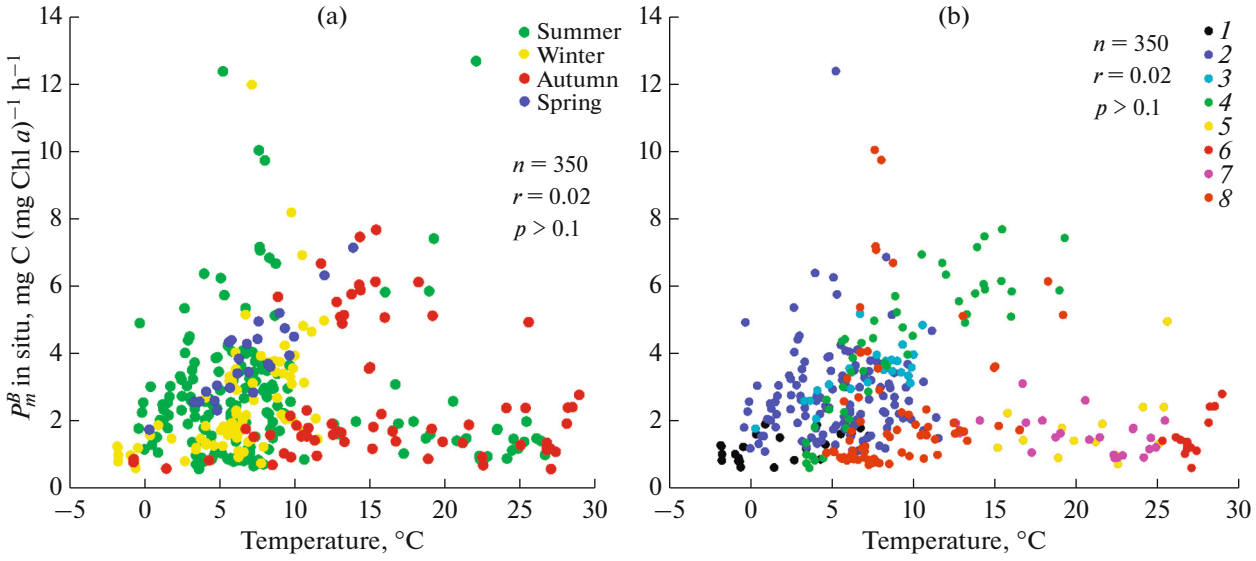

Fig. 2. Relationship between assimilation number (P_m^B) and sea surface temperature by (a) seasons and (b) area.

(July) [20]. Area 4 was characterized by moderately warm waters with an average Chl *a* concentration of 1.2 mg m^{-3} and maximum average P_m^B values of 4.2 mgC (mgChl *a*)$^{-1}$ h^{-1}. The measurements were likely carried out in this area at during the peak in phytoplankton (diatom) blooms (Table 1). Open ocean waters (areas 5–7) were distinguished by high SST (more than 20°C), low Chl *a* concentration (less than 1.2 mg m^{-3}), and relatively low P_m^B (1.6 mgC (mgChl *a*)$^{-1}$ h^{-1}, which was less than 4.9 mgC (mgChl *a*)$^{-1}$ h^{-1} in both spring and autumn (Fig. 2)), when diatoms and cyanobacteria dominated [20]. The measurements were carried out in this area in September–November during which time there were no blooms. In the southernmost region of the Atlantic Ocean considered (area 8), there was a high biomass indicative of diatoms (Table 1) and a temperature of 8.9°C, P_m^B was also relatively low (2.3 mgC (mgChl *a*)$^{-1}$ h^{-1}, on average).

Most P_m^B values were in the range of 0.5–4.1 mgC (mgChl *a*)$^{-1}$ h^{-1} at SST from 0°C to 11°C in the spring–summer period in areas 2, 4, and 8 (Fig. 2).

Relationship between P_m^B, temperature and chlorophyll *a* in the PANGAEA dataset. At all stations, the

Table 3. Statistical characteristics of assimilation number (P_m^B), sea surface temperature (SST), and chlorophyll *a* (Chl *a*) by seasons and area: mathematical equation ± standard deviation

Season/area	*N*	P_m^B, mgC (mgChl *a*)$^{-1}$ h^{-1}	SST, °C	Chl *a*, mg m^{-3}
Spring	179	2.65 ± 1.97	8.10 ± 6.61	2.12 ± 3.08
Summer	78	2.53 ± 1.79	6.13 ± 3.48	0.88 ± 0.71
Autumn	68	2.59 ± 1.95	15.99 ± 7.40	0.84 ± 0.82
Winter	25	3.85 ± 1.25	6.90 ± 2.88	0.72 ± 0.59
1	25	1.21 ± 0.40	2.04 ± 3.06	0.91 ± 0.74
2	129	2.76 ± 1.44	5.31 ± 2.84	2.24 ± 3.02
3	23	3.41 ± 0.79	7.23 ± 2.70	0.62 ± 0.48
4	47	4.16 ± 2.06	9.21 ± 4.51	1.20 ± 1.22
5	14	1.78 ± 1.06	20.97 ± 3.50	0.25 ± 0.21
6	15	1.51 ± 0.61	27.16 ± 0.96	0.21 ± 0.08
7	24	1.58 ± 0.55	20.25 ± 3.9	0.25 ± 0.33
8	69	2.33 ± 2.10	8.93 ± 3.26	1.83 ± 2.64
All stations	**350**	**2.70 ± 1.90**	**9.11 ± 6.94**	**1.50 ± 2.34**

Table 4. Dependence of assimilation number (P_m^B) on sea surface temperature (SST) and chlorophyll *a* (Chl *a*) by seasons and area. Significant correlation coefficients ($p < 0.05$ and $p < 0.01$) are highlighted in color

		SST and Chl *a*	P_m^B and SST	P_m^B and Chl-a
season/area	*N*	*r* (*p*-level)		
Spring	179	−0.23 ($p < 0.01$)	−0.05 ($p > 0.1$)	0.04 ($p > 0.1$)
Summer	78	0.22 ($p < 0.05$)	0.30 ($p < 0.01$)	−0.05 ($p > 0.1$)
Autumn	68	−0.60 ($p < 0.01$)	−0.03 ($p > 0.1$)	−0.08 ($p > 0.1$)
Winter	25	0.43 ($p < 0.05$)	0.82 ($p < 0.01$)	0.06 ($p > 0.1$)
1	25	0.60 ($p < 0.01$)	0.46 ($p < 0.05$)	−0.07 ($p > 0.1$)
2	129	0.01 ($p > 0.1$)	0.04 ($p > 0.1$)	0.06 ($p > 0.1$)
3	23	0.54 ($p < 0.01$)	0.67 ($p < 0.01$)	0.17 ($p > 0.1$)
4	47	−0.47 ($p < 0.01$)	0.86 ($p < 0.01$)	−0.61 ($p < 0.01$)
5	14	−0.92 ($p < 0.01$)	0.32 ($p > 0.1$)	−0.33 ($p > 0.1$)
6	15	−0.05 ($p > 0.1$)	0.35 ($p > 0.1$)	0.17 ($p > 0.1$)
7	24	−0.49 ($p < 0.05$)	−0.42 ($p < 0.05$)	0.08 ($p > 0.1$)
8	69	−0.09 ($p > 0.1$)	0.19 ($p > 0.1$)	0.02 ($p > 0.1$)
All stations	350	−0.22 ($p < 0.01$)	0.02 ($p > 0.1$)	0.01 ($p > 0.1$)

correlation between P_m^B, SST and Chl *a* was low (hereinafter, the correlation is considered according to the classification given in [2]): $n = 350$, $r = 0.02$ at $p > 0.1$ and $r = 0.01$ at $p > 0.1$, respectively. When these parameters were analyzed by season and region, the correlation coefficient for individual cases increased, but of course N was lower and the error is therefore potentially higher (Table 4).

In summer, the relationship between P_m^B and SST was significant, but moderate ($r = 0.30$ at $p < 0.01$) and nonlinear (Fig. 2a; Table 4). In winter, the P_m^B–SST relationship was higher ($r = 0.82$ at $p < 0.01$), and linear, with higher SST values causing an increase in P_m^B (Fig. 2a; Table 4). In the spring and autumn periods, no significant relationships were observed between these two parameters. No correlation with a Chl *a* was found in any season. By comparison, the SST–Chl *a* relationship was significant in all seasons: in spring and autumn, it was inverse, but weak; in autumn and winter, it was moderate and average: $r = 0.43$ for $p < 0.05$ and $r = -0.60$ for $p < 0.01$, respectively.

The areal division made it possible to identify a significant relationship between P_m^B and SST in four areas (Table 4): in area 1, the relationship was moderate ($r = 0.46$ at $p < 0.05$); in area 3, medium ($r = 0.67$ at $p < 0.05$); in area 4, high between P_m^B and SST and moderate with Chl *a* ($r = 0.86$ and $r = -0.61$, respectively). In this case, the relationship between P_m^B and SST was linear mainly between 3 and 10°C and nonlinear at SST > 10°C (Fig. 5a). In the open ocean, a significant relationship between P_m^B and SST only occurred in area 7 (Table 4). Most likely, the P_m^B–SST relationship is influenced by the phytoplankton bloom since in areas 1, 3, and 4, the measurements were made during the bloom period (Table 1), and the P_m^B–SST relationship was significant. By contrast, in area 8 where there was no bloom, even though the other environmental conditions were similar to area 4, no such relationship was observed.

Development of regional algorithm based on AMT-29 data. The AMT-29 data collected during autumn were then used to analyze the dependence of P_m^B on SST and Chl *a* separately. The analysis made it possible to reveal a significant relationship between P_m^B and SST ($r = 0.75$ at $p < 0.01$): an increase in SST resulted in higher P_m^B (Fig. 3). P_m^B was highest from the Equator to the Northern Tropics, and it was lowest within the Southern Subtropical Gyre (30°–40° S) (Fig. 1a). The P_m^B–Chl *a* relationship was in turn significant, moderate and inverse ($r = -0.61$ at $p < 0.1$). With increasing temperature (from 10 to 28°C) at low Chl *a* concentrations (0–1.5 mg m^{-3}), the P_m^B values increased (Fig. 3).

This relationship was used to develop a regional (for the Atlantic Ocean) empirical algorithm ($r^2 = 0.56$ at $p < 0.01$) for obtaining P_m^B as a function of SST and Chl *a* in the form of a multiple linear regression equation (*MY-21*):

$$P_m^B = -1.71 + 0.22T + 0.43\text{Chl } a, \quad (1)$$

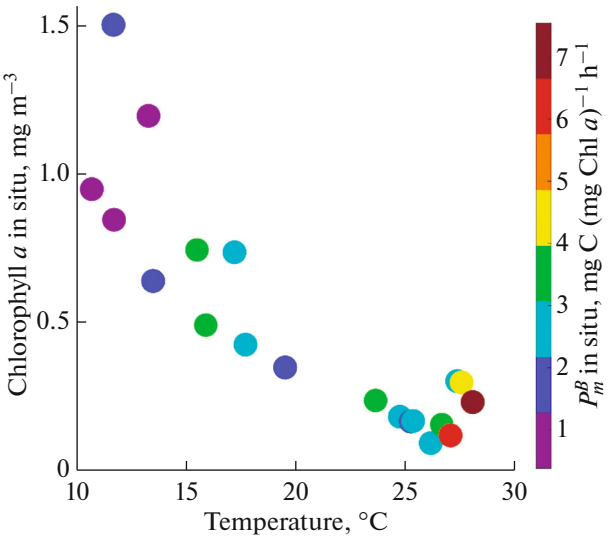

Fig. 3. Relationship between assimilation number (P_m^B), water temperature, and chlorophyll *a* concentration in surface waters ($n = 20$).

where T is water temperature (°C), and *Chla* is the Chl *a* concentration (mg m^{-3}). This algorithm was tested based on the data used to create it (calibration), and the model values were revealed to have a slight deviation from the factual ones: the systematic error (SE) was 0.005 (mgC (mgChl *a*)$^{-1}$ h^{-1}), the average absolute error was 0.95 (mgC (mgChl *a*)$^{-1}$ h^{-1}), and the absolute percentage error (APE) was 44%.

Development of regional algorithm using the PANGAEA data. The algorithms were developed to predict P_m^B as a function of SST by season (summer and winter) and region (1, 3, and 4) using a test sample set (Fig. 1b). The coefficients of the equation were obtained using Matlab R2019a ("fitlm" function, "cftool" package). The algorithms are first-order linear equations:

$$P_m^B = A + BT, \quad (2)$$

where A, B are the selected coefficients.

The algorithms were developed for areas with significant P_m^B–SST relationships (Table 4) and where test sample data were available. Linear regression equations were used to create the algorithms. The coefficients of the algorithms by area and their accuracy are given in Table 4.

Area 4 is considered in detail below, although the accuracy of the P_m^B algorithm is lower than for area 3 ($r^2 = 0.29$ and $r^2 = 0.37$, respectively) (Table 5). Area 4 was validated using a greater number of stations in the main sampling set ($n = 47$ and 23, respectively) (Table 1), while the P_m^B–SST relationship in this area was the highest ($r = 0.86$) of all areas tested (Table 4). The accuracy of the P_m^B algorithm developed for area 1 was low (Table 5).

Using the test sampling set used to develop the algorithm, the P_m^B–SST relationship was moderate in area 4, which had temperatures between 8 and 11°C, and in which P_m^B varied over a wide range (1–8 mgC (mgChl *a*)$^{-1}$ h^{-1}) (Fig. 4a). When comparing the model and in situ data on the scatter diagram, the algorithm yielded the following results for area 4: the regression and correspondence lines were almost coincident ($a = 1.06$ and $b = 0.08$) (Fig. 4b) with an algorithm accuracy of 29% ($r^2 = 0.29$).

DISCUSSION

***P_m^B*–temperature relationship.** The relationships between physico-chemical environmental conditions and P_m^B observed in this study, partially confirm the earlier findings that water temperature can be a good predictor of P_m^B only in the coastal and temperate oceanic regions (Table 4). In these regions, temperature can be a major factor in the successional changes of the phytoplankton community [12, 15, 29]. The optimum temperature conditions for increasing P_m^B usually do not exceed 20°C due to growth rate features of phytoplankton cells and the functioning of Calvin cycle enzymes [7, 28, 30]. This trend is observed in the dynamically active areas: 3, the Labrador Sea and 4, the Bank of Newfoundland (Fig. 2b). In area 4, a linear increase in P_m^B was observed in SST from 3 to 10°C, when the P_m^B–SST relationship was nonlinear (Fig. 5a). As for colder waters (BPLR, ARCT, SARC, and

Table 5. Regional empirical algorithms developed for the assimilation number. The accuracy of each algorithm is expressed in terms of determination coefficient (r^2). P_m^B is assimilation number, and T is sea surface temperature

Area	Algorithm	Accuracy of algorithm, r^2
Area 1, $n = 37$	$P_m^B = 0.06T + 1.08$	0.13
Area 3, $n = 34$	$P_m^B = 0.21T + 1.82$	0.37
Area 4, $n = 53$	$P_m^B = 0.38T + 0.75$	0.29

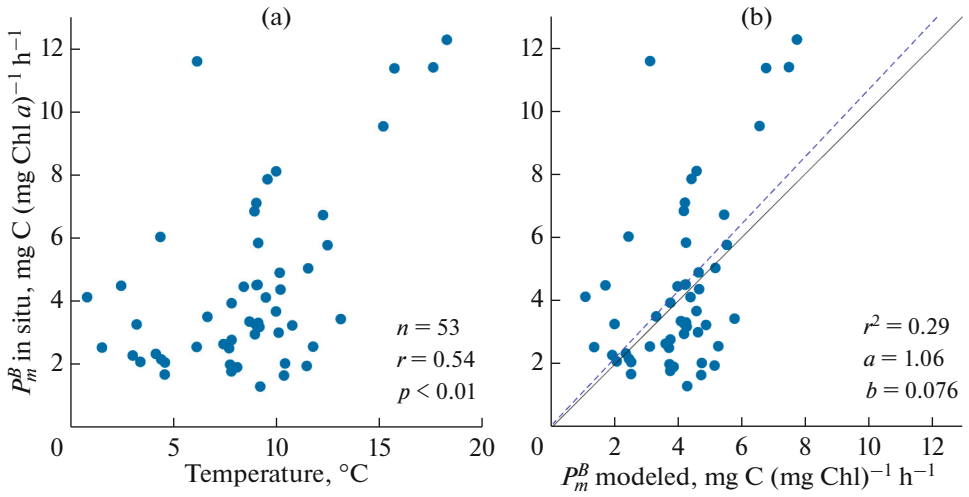

Fig. 4. Scatter diagrams for area 4 based on test sample data: (a) dependence of in situ P_m^B on water temperature and (b) comparison of modeled estimates with in situ data. Solid line is correspondence line (1 : 1); dotted line is linear regression line.

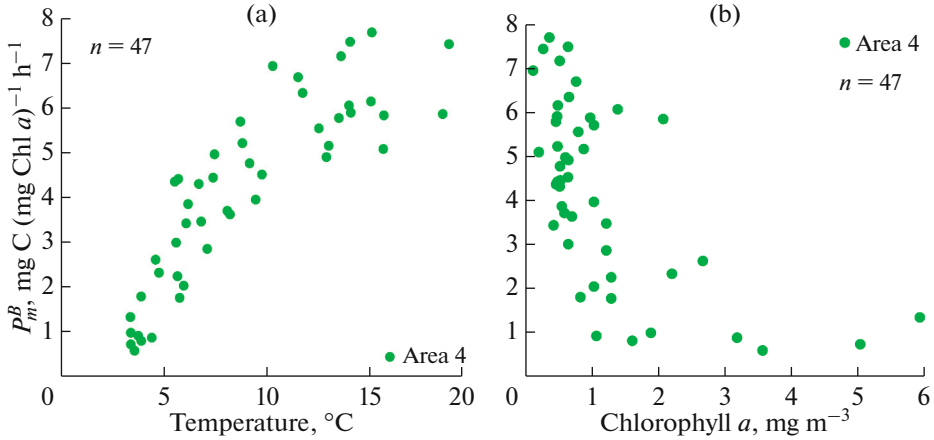

Fig. 5. Relationship of assimilation number (P_m^B) with (a) water temperature and (b) chlorophyll a concentration in area 4.

FKLD provinces), where SST does not exceed 10°C, no dependence was detected and there was a very wide range in P_m^B values (Fig. 2b). Low P_m^B values at SST > 20°C are probably caused by a lack of N combined with a higher energy phytoplankton consumption for photoprotection under a high surface irradiance, which is characteristic of stratified oligotrophic waters [7, 16, 27]. When SST is more than 12°C, two regional variants for P_m^B variations are possible: the values reach 5–7 mgC (mgChl a)$^{-1}$ h^{-1} at 40° N, and they do not exceed 3 mgC (mgChl a)$^{-1}$ h^{-1} at SST of 15–29°C in the open part of the ocean. In both cases, the measurements were carried out in the spring and autumn bloom periods (Table 1). In areas 5–7 (open waters of the southern part of the Atlantic region), such low P_m^B values are natural, because it is a tropical and subtropical region where the surface layer is characterized by low N and a high solar radiation: all phytoplankton energy is used in photoadaptation [27].

A significant P_m^B–SST relationship was recorded in areas 1, 3, 4, and 7 (0.46, 0.67, 0.86, and –0.42, respectively) (Table 4). Positive correlations in the ecosystems of temperate latitudes were noted earlier [26, 29] and were justified by the temperature effect on the phytoplankton community structure (size and taxonomic composition) [11]. If water temperature is an indicator of low N waters, as in the case of area 7 (the center of the Southern Subtropical Gyre), which is a convergence zone, the P_m^B–SST relationship will be negative, because a depletion in N is a photosynthetic limiting factor [18, 32].

In one of the latest studies [19], the average P_m^B–SST correlation value did not exceed 0.42 in different

parts of the Global Ocean. These data are indicative of the fact that SST alone is not enough to fully describe the variability in P_m^B. In this case, the estimation of P_m^B should also take into account other factors such as light, N availability, and the size composition of the phytoplankton community.

P_m^B–Chl *a* relationship based on pangaea and AMT-29 data. It is noteworthy that for Chl *a* concentrations > 1 mg m^{-3}, P_m^B is low (less than 4 mgC (mgChl *a*)$^{-1}$ h^{-1}), while at a low biomass, when the phytoplankton community structure can be mixed, P_m^B is highly variable. These data correspond to the observations in [11, 24, 26] and are explained by the fact that low Chl *a* concentrations can result from the combined action of unfavorable external factors: low illumination, limited *N*, and an increase in the zooplankton population. Each of these factors influences the phytoplankton ability to photosynthesis: colder waters of high latitudes subjected to a vertical mixing several times during the year (autumn/spring convention) are enriched in *N* (areas 1 and 2) [12, 26]. In these waters, the phytoplankton community structure contains larger cells (e.g., diatoms) compared to more southern waters and contributes to a higher phytoplankton biomass [4, 26]. P_m^B is low however (Table 3), because solar radiation is not sufficient for intensive photosynthesis during the production period. In temperate waters (areas 3, 4, and 8), SST values are higher, solar energy is greater, nanophytoplankton is predominant, biomass is slightly lower than in the northern regions, and P_m^B tends to be higher (Table 3) [12, 13, 26]. Warm, consistently stratified oligotrophic waters (areas 5–7) with a high solar radiation throughout the year are dominated by a smaller abundance of phytoplankton (cyanobacteria), and, accordingly, are characterized by low biomass and P_m^B due to a lack of N and an excessive illumination (Table 3) [11–14, 26].

A significant (negative) relationship between P_m^B and the Chl *a* concentration was determined only in area 4 (Bank of Newfoundland) in April–May and October–December ($r = -0.61$ for $p < 0.01$) (Fig. 5b), according to the PANGAEA data, and during the run of the AMT-29 research vessel ($r = -0.61$ at $p < 0.01$) in the autumn period. No significant P_m^B–Chl *a* relationship was observed in most areas of the Atlantic Ocean, as was noted in previous studies [19].

Validation of temperature based algorithms for obtaining P_m^B. As mentioned above, a significant P_m^B–SST relationship, from moderate to high, was determined in certain areas of the Atlantic Ocean (Table 4): area 1, $r = 0.45$; area 3, $r = 0.67$; and area 4, $r = 0.86$. Regional linear algorithms for obtaining P_m^B were developed (Table 5) for these areas based on the PANGAEA data set ($n = 141$, Fig. 1b). A subset of the data was used to validate the algorithm (*MY-22*), *MY-21* and other temperature algorithms were also used in the PP reconstruction models (Table 2).

The dynamically active region 4 ($n = 47$, Gulf Stream turn, Bank of Newfoundland) is considered in detail below (Figs. 6, 7; Table 6). This area is characterized by moderately warm waters (3.4–19.3°C) with an average Chl *a* concentration of 1.2 mg m^{-3} and maximum P_m^B among the average values of the Atlantic Ocean (4.2 mgC (mgChl *a*)$^{-1}$ h^{-1}). In addition to the high P_m^B–SST relationship, this is the only area with a significant relationship between P_m^B and Chl *a* concentration ($r = -0.61$ at $p < 0.01$). The model values of the algorithms were closely related to in situ P_m^B ($r > 0.70$ in absolute value); the exception was the *MY-21* algorithm characterized by the lowest correlation with the initial data, which resulted in a considerable underestimation and the highest deviation angle of the linear regression line (Fig. 6). Model *BB* estimates deviated from the real values to the greatest extent (root mean square error (RMSE) of up to 4.23 (Fig. 7); APE = 195%). In addition, *BB* overestimated P_m^B (SE = 1.38), while the linear regression line had the smallest slope compared to other algorithms (Fig. 6). The *M* algorithm estimates of P_m^B were in a relatively narrow range (1.8–2.5 mgC (mgChl *a*)$^{-1}$ h^{-1}), and were several times less than the actual P_m^B. The *BF* and *MY-22* algorithms led to a similar distribution of points however, the regionally selected algorithm (*MY-22*) had a smaller linear regression line angle (Fig. 6); the standard deviation (SD) was closer to the in situ SD (Fig. 7), and the deviations of the model estimates were low: SD = 1.03, SE = –0.01, and APE = 36%. The *MY-22* algorithm was distinguished by the minimum difference in terms of SD and the minimum RMSE value out of the three algorithms (*BF*, *M*, and *MY-22*) aligned almost in one line according to the correlation coefficient in Fig. 7.

In addition to these algorithms, we should note other suitable algorithms for each of three regions: the *M* algorithm is also suitable for cold area 1 with low P_m^B; the *BF* and *M* algorithms are suitable for areas 3 and 4, where P_m^B was maximum at moderate water temperatures (Table 6).

Based on our results, accounting for the photoperiod does not contribute to more accurate estimates of P_m^B: the *BB* algorithm leads to relatively high overestimates of the in situ values. It should be noted that the P_m^B dependence on SST in this algorithm is exponential [6, 7]: the authors assumed that P_m^B would decrease when moving from water areas with cold

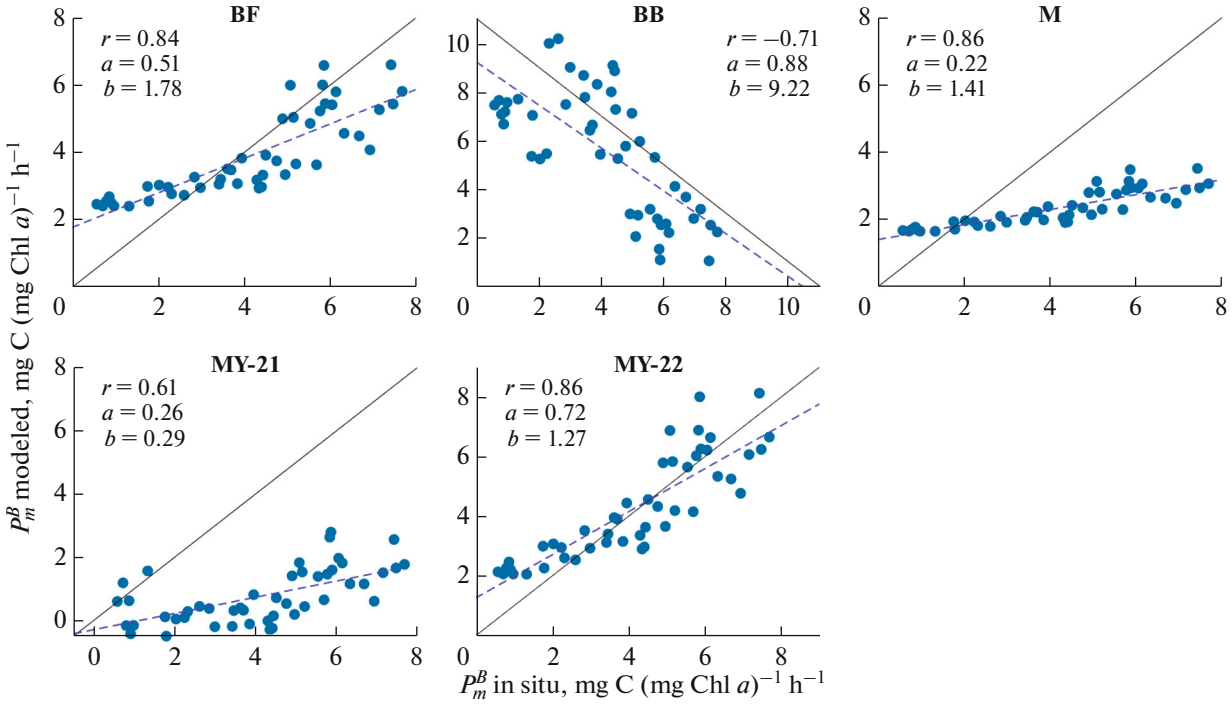

Fig. 6. Scatter diagrams of model and in situ P_m^B for area 4, $n = 47$. Solid line is correspondence line (1 : 1); dotted line is linear regression line.

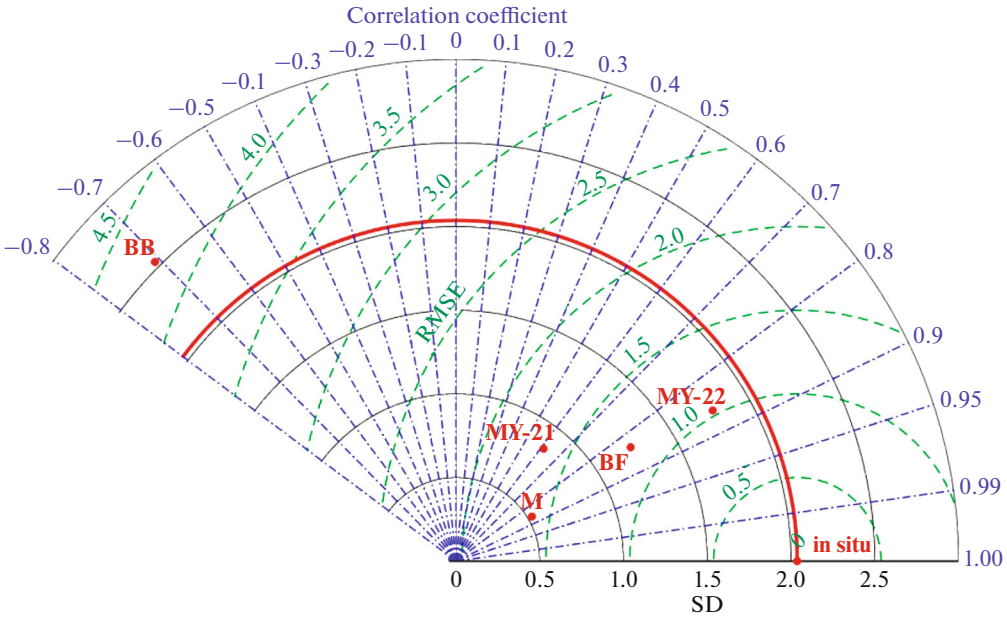

Fig. 7. Taylor diagram for modeled and in situ P_m^B (mgC (mgChl a)$^{-1}$ h^{-1}) in area 4, $n = 47$. Dashed blue lines with dot designate r (correlation coefficient); solid arcs are SD; and dotted green lines are RMSE.

N-saturated waters and longer daylight hours to those with warm oligotrophic water, lack of N, and shorter daylight hours [6]. The excess of model P_m^B estimates over the in situ data was also noted by the authors of the *BB* algorithm [6].

The use of the Chl *a* concentration in the P_m^B algorithms, in turn, makes sense in the areas where P_m^B is closely related to this parameter (area 4) (Table 4). The idea of joint use of the phytoplankton biomass and SST, which can be estimated remotely, to determine

Table 6. Estimated statistical relationship between modeled and in situ assimilation number (P_m^B) (mgC (mgChl *a*)$^{-1}$ h^{-1}) in areas 1, 3, and 4. Mathematical statistics: SD (Standard Deviation), RMSE (Root Mean Square Error), SE (Systematic Error), and APE (Absolute Percentage Error, %). Most significant statistical values are highlighted in grey

	SD	*r*	*p*-level	RMSE	SE	APE
in situ P_m^B	0.40	Area 1, $n = 25$				
BF	0.83	0.48	$p < 0.05$	0.71	0.76	74
BB	1.95	–0.50	$p < 0.05$	2.14	4.65	473
M	0.37	0.46	$p < 0.05$	0.38	0.28	40
MY-21	0.89	0.31	$p > 0.1$	0.82	–2.09	191
MY-22	0.20	0.46	$p < 0.05$	0.34	0.03	27
in situ P_m^B	0.79	Area 3, $n = 23$				
BF	0.65	0.67	$p < 0.01$	0.54	–0.14	11
BB	5.51	–0.71	$p < 0.01$	5.92	2.93	148
M	0.32	0.67	$p < 0.01$	0.59	–1.31	37
MY-21	0.70	0.56	$p < 0.01$	0.64	–3.30	100
MY-22	0.56	0.67	$p < 0.01$	0.54	–0.08	10
in situ P_m^B	2.06	Area 4, $n = 47$				
BF	1.26	0.84	$p < 0.01$	1.21	–0.25	46
BB	2.56	–0.71	$p < 0.01$	4.23	1.38	195
M	0.53	0.86	$p < 0.01$	1.61	–1.83	52
MY-21	0.86	0.61	$p < 0.01$	1.66	–3.38	83
MY-22	1.80	0.86	$p < 0.01$	1.03	–0.01	35

P_m^B was proposed earlier [26]. The multiple linear regression analysis made it possible to show that SST, as the only predictor, largely explains the variability in P_m^B ($r^2 = 0.56$, $n = 477$) and adding the logarithmic Chl *a* concentration does not greatly increase the correlation when validating the algorithm ($r^2 = 0.57$, $n = 472$). In this study, P_m^B obtained from the multiple linear regression equation using SST and Chl *a* (*MY-21*) does not fit the in situ P_m^B well in area 1 (Northeast Greenland waters). This can be explained by the environmental conditions, which do not correspond to those at the stations used in the algorithm developed.

In conclusion, the results obtained in this study agree with the earlier studies that P_m^B algorithms based on temperature can describe the variability in P_m^B up to 20–45% [7, 19, 23], and in individual regions of the Global Ocean, up to 60% [26]. In addition, the simple linear temperature algorithms of P_m^B proposed in this study (*MY-22*) are more efficient than the seventh-order polynomial (*BF*), and the fitted region-specific linear equation coefficients provide the closest estimates to in situ P_m^B.

CONCLUSIONS

This study assessed the variability in P_m^B in different areas of the Atlantic Ocean that have both different temperatures and phytoplankton species. Algorithms of P_m^B were developed based on linear relationships with temperature and chlorophyll *a*. The highest P_m^B values were found in area 3, the Labrador Sea where SST = 7.2 ± 2.7°C; area 4, Bank of Newfoundland where the average SST = 9.2 ± 4.5°C. Both of the areas were dominated by diatoms. In both regions and by season, P_m^B was more highly correlated with SST than chlorophyll *a*. The analysis of the correlation relationship showed that P_m^B is more correlated with SST than with chlorophyll *a*, both in the parts of the Atlantic Ocean under study and in the analyzed seasons as a whole. In connection with the above, the development of regional algorithms using satellite data was based on the temperature dependence.

New regional algorithms for P_m^B as a function of SST were therefore developed for areas 1, 3, and 4 (Arctic latitudes, Labrador Sea, Bank of Newfoundland), and were compared with other algorithms that already exist for P_m^B and P_{opt}^B. The new regional empir-

ical algorithm was closer to the in situ data, despite their simplicity and in the absence of other input parameters. This was because these algorithms were developed for specific areas and account for the local range in P_m^B. In addition, P_m^B most closely correlated with SST ($r = 0.46–0.86$) in these areas and can therefore be used easily with ocean remote sensing data. Using regional empirical coefficients, these algorithms explain 21–74% of the variability in P_m^B.

ACKNOWLEDGMENTS

The authors thank the Plymouth Marine Laboratory (Plymouth, UK) for the opportunity to obtain data on the specific maximum rate of photosynthesis. We are grateful to the Principal Scientific Officer, Dr. Giorgio Dall'Olmo on AMT-29 and to Anakha Mohan for providing the water temperature and chlorophyll *a* concentration data.

FUNDING

The research of Russian scientists was supported by the Ministry of Science and Higher Education of the Russian Federation (project no. 13.2251.21.0006, agreement no. 075-10-2021-104, Electronic Budget Information System). Dr. Gavin Tilstone was supported by the UK Natural Environment Research Council (NERC) National Capability funding to Plymouth Marine Laboratory for the Atlantic Meridional Transect.

ETHICS APPROVAL AND CONSENT TO PARTICIPATE

This work does not contain any studies involving human and animal subjects.

CONFLICT OF INTEREST

The authors of this work declare that they have no conflicts of interest.

REFERENCES

1. G. P. Berseneva and E. A. Kuftarkova, "Seasonal dynamics of the main physiological indicators of phytoplankton in coastal deformed ecosystems," Ekol. Morya **41**, 28–32 (1992).
2. E. V. Ivanter and A. V. Korosov, *Fundamentals of Biometrics: Introduction to Statistical Analysis of Biological Phenomena and Processes* (Izd. Petrozavodsk. Gos. Univ. 1992) [in Russian].
3. A. S. Malysheva and P. V. Lobanova, "Restoration of the maximum specific rate of photosynthesis as a function of water temperature and chlorophyll-a in water areas with different oceanological conditions using the example of the Atlantic Ocean," in *Comprehensive Studies of the World Ocean. Materials of the VI All-Russian Scientific Conference of Young Scientists, Moscow, April 18–24, 2021* (Shirshov Inst. Oceanol. Russ. Acad. Sci., Moscow, 2021), pp. 511–512.
4. L. A. Pautova, A. B. Demidov, V. A. Silkin, et al., "Coccolithophores in summer phytoplankton of the Irminger Sea," in *Geology of Seas and Oceans. Proceedings of the XXIII International Scientific Conference (School) on Marine Geology* (2019), pp. 188–189.
5. Z. Z. Finenko, T. Ya. Churilova, H. M. Sosik, and O. Basturk, "Variability of photosynthetic parameters of the surface phytoplankton in the Black Sea," Oceanology **42** (1), 53–67 (2002).
6. W. Balch, R. Evans, J. Brown, et al., "The remote sensing of ocean primary productivity—use of a new data compilation to test satellite algorithms," J. Geophys. Res. **97**, 2279–2293 (1992).
7. M. Behrenfeld and P. Falkowski, "Photosynthetic rates derived from satellite-based chlorophyll concentration," Limnol. Oceanogr. **42** (1), 1–20 (1997).
8. M. J. Behrenfeld, E. Marañón, D. A. Siegel, and S. B. Hooker, "Photoacclimation and nutrient-based model of lightsaturated photosynthesis for quantifying oceanic primary production," Mar. Ecol. Prog. Ser. **228**, 103–117 (2002).
9. H. A. Bouman, T. Platt, M. Doblin, et al., "Photosynthesis–irradiance parameters of marine phytoplankton: Synthesis of a global data set," Earth Syst. Sci. Data **10**, 251–266 (2018).
10. H. A. Bouman, T. Platt, M. A. Doblin, et al., "A global dataset of photosynthesis-irradiance parameters for marine phytoplankton," Pangaea, 874087 (2017).
11. H. A. Bouman, T. Platt, S. Sathyendranath, et al., "Temperature as indicator of optical properties and community structure of marine phytoplankton: Implications for remote sensing," Mar. Ecol. Prog. Ser. **258**, 19–30 (2003).
12. H. A. Bouman, T. Platt, S. Sathyendranath, and V. Stuart, "Dependence of light-saturated photosynthesis on temperature and community structure," Deep-Sea Res. I **52** (7), 1284–1299 (2005).
13. V. Brotas, G. A. Tarran, V. Veloso, et al., "Complementary approaches to assess phytoplankton groups and size classes on a long transect in the Atlantic Ocean," Front. Mar. Sci. **8**, 682621 (2022). https://doi.org/10.3389/fmars.2021.682621
14. M.-E. Carr, M. A. M. Friedrichs, M. Schmeltz, et al., "A comparison of global estimates of marine primary production from ocean color," Deep-Sea Res. II **53** (5), 741–770 (2006).
15. R. W. Eppley, "Temperature and phytoplankton growth in the sea," Fish. Bull. **70** (4), 1063–1085 (1972).
16. R. Geider, H. MacIntyre, and T. Kana, "Dynamic model of phytoplankton growth and acclimation: Responses of the balanced growth rate and the chlorophyll a carbon ratio to light, nutrien-limitation and temperature," Mar. Ecol. Prog. Ser. **148**, 187–200 (1997).
17. W. G. Harrison and T. Platt, "Variations in assimilation number of coastal marine phytoplankton: Effects of environmental co-variates," J. Plankton Res. **2**, 249–260 (1980).
18. D. Kamykowski, S. J. Zentara, J. M. Morrison, and A. C. Switzer, "Dynamic global patterns of nitrate, phosphate, silicate, and iron availability and phytoplank-

ton community composition from remote sensing data," Glob. Biogeochem. Cycles **16**, 25-1–25-29 (2002).

19. G. Kulk, T. Platt, J. Dingle, et al., "Primary production, an index of climate change in the ocean: satellite-based estimates over two decades," Remote Sens. Environ. **12** (5), 826–846 (2020).
20. A. R. Longhurst, *Ecological Geography of the Sea*, 2nd ed. (Elsevier Academic Press, 2007).
21. H. L. MacIntyre, T. M. Kana, T. Anning, and R. Geider, "Photoacclimation of photosynthesis irradiance response curves and photosynthetic pigments in microalge and cyanobacteria," J. Phycol. **38**, 17–38 (2002).
22. R. O. Megard, "Phytoplankton, photosynthesis, and phosphorus in Lake Minnetonka, Minnesota," Limnol. Oceanogr. **17** (1), 68–87 (1972).
23. S. Milutinović and L. Bertino, "Assessment and propagation of uncertainties in input terms through an ocean-color-based model of primary productivity," Remote Sens. Environ. **115** (8), 1906–1917 (2011).
24. T. Platt, H. Bouman, E. Devred, et al., "Physical forcing and phytoplankton distributions," Scientia Marina **69**, 55–73 (2005).
25. T. Platt and S. Sathyendranath, *Modelling Marine Primary Production* (Halifax, Nova Scotia, 2002).
26. T. Platt, S. Sathyendranath, M.-H. Forget, et al., "Operational estimation of primary production at large geographical scales," Remote Sens. Environ. **112** (8), 3437–448 (2008).
27. J. A. Raven, "The cost of photoinhibition," Physiol. Planta **142**, 87–104 (2011).
28. J. A. Raven and R. J. Geider, "Temperature and algal growth," New Phytol. **110**, 441–461 (1988).
29. K. Richardson, J. Bendtsen, T. Kragh, and E. A. Mousing, "Constraining the distribution of photosynthetic parameters in the global ocean," Front. Mar. Sci. **3** (2016).
30. A. Robinson, H. A. Bouman, G. H. Tilstone, and S. Sathyendranath, "Size class dependent relationships between temperature and phytoplankton photosynthesis-irradiance parameters in the Atlantic Ocean," Front. Mar. Sci. **4**, 435 (2018).
31. S. V. Rodrigues, M. M. Marinho, C. C. Cubas Jonck, et al., "Phytoplankton community structures in shelf and oceanic waters off southeast Brazil (20°–25° S), as determined by pigment signatures," Deep-Sea Res. I **88**, 47–62 (2014).
32. S. Sathyendranath, T. Platt, E. P. W. Horne, et al., "Estimation of new production in the ocean by compound remote-sensing," Nature **353**, 129–133 (1991).
33. S. Saux-Picart, S. Sathyendranath, M. Dowell, et al., "Remote sensing of assimilation number for marine phytoplankton," Remote Sens. Environ. **146**, 87–96 (2014).
34. G. H. Tilstone, B. H. Taylor, D. Blondeau-Patissier, et al., "Comparison of new and primary production models using SeaWiFS data in contrasting hydrographic zones of the northern North Atlantic," Remote Sens. Environ. **156**, 473–489 (2015).

Translated by E. Maslennikova